AUTHOR(S):

Seniorita, Latifa; Minami, Eiji; Yazawa, Yoshiteru; Hitoshi, Hayashi; Saka, Shiro

Title: Differential scanning calorimetric study of solidification behavior of monoglycerides

to investigate cold-flow properties of biodiesel

Running title: Thermodynamics of binary monoglycerides

Authors: Latifa Seniorita[1], Eiji Minami[1], Yoshiteru Yazawa[2], Hitoshi Hayashi[2], Shiro Saka[1]

Affiliations:

1. Graduate School of Energy Science, Kyoto University, Japan

2. Material Engineering Division No.2, Toyota Motor Corporation, Japan

Corresponding author: Eiji Minami

Address: Graduate School of Energy Science, Kyoto University, Yoshida-honmachi,

Sakyo-ku, Kyoto 606-8501, Japan

Tel/Fax: +81 (0)75 753 5713

E-mail: minami@energy.kyoto-u.ac.jp

1   **Abstract:**

2   Monoglycerides (MGs) are impurities present in biodiesel as a result of incomplete reactions.

3   MGs often solidify in biodiesel even at room temperature because of their high melting

4   points. This worsens the cold-flow properties such as the cloud point and pour point. We

5   hypothesized that several types of MGs solidify simultaneously; therefore we performed

6   differential scanning calorimetry of binary mixtures of MGs to elucidate their interactions

7   during solidification. Three thermodynamic formulas were then applied to the experimental

8   results: 1) non-solid-solution, 2) solid-solution, and 3) compound formation models. Binary

9   mixtures of MGs showed complicated liquidus curves with multiple upward convex shapes,

10   with which only the compound formation model fitted well. This model was applied to

11   multi-component mixtures that consisted of MGs and fatty acid methyl esters as surrogate

12   biodiesel fuels. We confirmed that the model still worked well. The results show that the

13   compound formation model has good potential for predicting the cold-flow properties of

14   biodiesel.

15

16   **Keywords:** Biodiesel, Polymorphism, Thermal analysis

17

18

19

Introduction

20

21   Biodiesel is a mixture of fatty acid methyl esters (FAMEs), which are produced by

22   transesterification of plant oils, and is used as a fossil diesel substitute. It is renewable and

23   has a low sulfur content but poor cold-flow properties (CFPs) compared with those of fossil

24   diesel. The CFPs such as the cloud point and pour point determine the low-temperature

25   fluidity of a liquid fuel. Prediction of biodiesel CFPs is therefore important for minimizing

26   the risk of fuel clogging.

27   Many models for predicting biodiesel CFPs have been reported (Imahara et al.,

28   2006; Lopes et al., 2008; Sarin et al., 2009; Coutinho et al., 2010; Dunn, 2010). Saturated

29   FAMEs such as methyl palmitate greatly affect the CFPs because of their high melting points

30   (Dunn and Bagby, 1995; Knothe, 2005). Sarin et al. (2009) established regression formulas

31   for predicting the cloud point and pour point as a linear function of methyl palmitate content

32   for biodiesel fuels from palm (*Elaeis guineensis*), jatropha (*Jatropha curcas*), and pongamia

33   (*Pongamia pinnata*) oils. Such empirical models are simple and easy to use, but not

34   applicable to biodiesel fuels from other feedstocks because the fatty acid compositions are

35   different. Some research groups have investigated thermodynamic models that are applicable

36   to any biodiesel (Imahara et al., 2006; Lopes et al., 2008; Coutinho et al., 2010). Imahara et

37   al. (2006) calculated the solid–liquid equilibria of FAME mixtures, with the assumption of

38   ideal liquid solutions, and found that the theoretical liquidus temperatures were in good

3

39 agreement with the experimental cloud points. The liquidus temperature is defined as the

40 temperature above which a given mixture is completely in the liquid phase. A solid phase can

41 form when the mixture is cooled below the liquidus temperature, therefore it is an important

42 index for predicting CFPs.

43   The thermodynamic models (Imahara et al., 2006; Lopes et al., 2008; Coutinho et al.,

44 2010) were based on the theory of solid-liquid equilibrium, where the fugacity of each

45 component is equal in solid and liquid phases. This theory expresses the relationship between

46 the liquidus temperature and properties of the mixture, such as chemical composition,

47 melting point and enthalpy of fusion of each component. The liquidus temperature is thus

48 predicted from the properties of the mixture. The theory is well described in a textbook of

49 chemical physics (Smith et al., 2005).

50   The presence of minor components also considerably affects the CFPs.

51 Monoglycerides (MGs), which are intermediate compounds produced during

52 transesterification, are typical minor components in biodiesel, and the European standard

53 restricts the total amount of MGs to below 0.8 wt% (Committee for Standardization

54 Automatic Fuels, 2008). MGs occasionally solidify even at around room temperature because

55 their melting points are high (Tang et al., 2008; Chupka et al., 2011; Chupka et al., 2014).

56 MGs have various crystalline structures, namely α, β′, and β types, and each has a different

57 melting point in the following order, α < β′ < β (Fischer et al., 1920; Malkin and Shurbagy,

4

58   1936). In general, α-type crystals form first when a liquid MG is cooled until the phase

59   transition occurs. The α crystals are converted irreversibly to the β′ type and then to the β

60   type after specific transition times (Maruyama et al., 1973). The potential presence of several

61   polymorphs makes the solidification behavior of MGs complicated. Chupka et al. studied the

62   effects of MGs on biodiesel CFPs and highlighted the importance of MG polymorphism

63   (Chupka et al., 2011; Chupka et al., 2014).

64   Our research group previously developed a thermodynamic model for calculating

65   the solid–liquid equilibria of surrogate biodiesel fuels containing MGs (Yoshidomi et al.,

66   2017; Sugami et al., 2017). We found that a binary mixture of a MG and a FAME behaves as

67   a non-ideal liquid solution because of the large difference between the chemical structures of

68   the components, and the non-ideality is well described by a modified version of the universal

69   quasi-chemical functional-group activity coefficients (UNIFAC) model, known as the

70   UNIFAC (Dortmund) model (Gmehling et al., 1993). When the mixture contains only one

71   type of MG, the predicted values are in excellent agreement with the experimental results.

72   However, deviations arise when the mixture includes two different MGs (Yoshidomi et al.,

73   2017; Sugami et al., 2017). We hypothesized that this discrepancy is caused by

74   co-crystallization (solid solution) of the different MGs, because our previous model assumed

75   that the solid phase consists of a single component. Lutton and Jackson (1967) and

76   Maruyama et al. (1978) have reported the formation of such solid solutions of different MGs

5

77   under certain conditions.

78   The aim of the current study was to use differential scanning calorimetry (DSC) to

79   investigate the interactions between MGs and to develop an appropriate thermodynamic

80   model for describing the solidification behaviors of MGs. The model obtained was then

81   applied to multi-component mixtures, which contained two types of MGs in FAMEs and

82   served as surrogate biodiesel fuels. The results of this study will help to establish a

83   prediction model for real biodiesel, which contains several types of MGs.

84

85   **Experimental Procedures**

86   Materials

87   The MG samples used were 1-monolaurin (MG12:0, purity 99%, Tokyo Chemical

88   Industry, Tokyo, Japan), 1-monopalmitin (MG16:0, 99%, Olbracht Serdary Research

89   Laboratories (OSRL), Toronto, Canada), and 1-monostearin (MG18:0, 99%, OSRL). The

90   FAME samples were methyl laurate (FAME12:0, 99%), methyl palmitate (FAME16:0, 99.5%),

91   and methyl oleate (FAME18:1, 99%), which were all purchased from Sigma-Aldrich Japan,

92   Tokyo. Test samples for DSC were prepared by blending these chemicals in various ratios,

93   without purification.

94

95

96   Analytical methods

97   For DSC analyses, samples (about 10 mg) were placed in non-hermetic

98   aluminum-based pans under a dry nitrogen flow. Indium and zinc were used for temperature

99   calibration and α-alumina was used as a reference material. We determined the liquidus

100   temperature for each sample from the obtained DSC profile. Because MGs are polymorphic,

101   we used two different methods for examining α- and β-type crystals.

102   For α-type crystals, each sample was heated until fully melted and cooled until the

103   first exothermic peak was detected; the solid phase formed at this time is thought to consist

104   of α-type crystals (Maruyama et al., 1973; Yoshidomi et al., 2017). The sample was then

105   reheated immediately at a heating rate of 3 °C/min and the DSC profile was recorded. This

106   rapid heating prevents the crystal transition to the β′ or β type during analysis. For β-type

107   crystals, each solidified sample was held in a thermostatic chamber at 50 °C for four weeks to

108   ensure the transition to the β type, which is the most stable structure. The reported times for

109   transition to the β type are about 0.1, 100, and 230 h at 50 °C for MG12:0, MG16:0, and

110   MG18:0, respectively (Maruyama et al., 1971); four weeks (672 h) is therefore considered to

111   be sufficient. After removal from the chamber, the sample was exposed at room temperature

112   for a few minutes, and then DSC was performed at a heating rate of 1 °C/min.

113   For each pure MG, the melting point was estimated from the onset temperature of

114   the endothermic peak in the DSC profile. In the case of a binary or multi-component mixture,

115 the highest endothermic peak maximum temperature was defined as the experimental liquidus

116 temperature, as in previous studies (Maruyama et al., 1971; Knothe and Dunn, 2009;

117 Yoshidomi et al., 2017). Note that this is a rough estimate because the absolute liquidus

118 temperature is generally difficult to determine, especially for multi-component systems.

119

120 Thermodynamic models

121   Three thermodynamic models were used to calculate the liquidus temperatures. The

122 first two models were based on the solid–liquid equilibrium and the third was derived from

123 the reaction equilibrium. The calculations were conducted using programs coded with

124 Microsoft Visual Basic for Applications on Excel.

125

126 *Solid–liquid equilibrium*

127   At solid–liquid equilibrium, the fugacity of each component i in a given system is

128 the same in the solid (S) and liquid (L) phases; this relationship is expressed by the following

129 equation:

130 $$\gamma_i^{\mathrm{L}} x_i f_i^{\mathrm{L}} = \gamma_i^{\mathrm{S}} z_i f_i^{\mathrm{S}} \tag{1}$$

131 where x_i and z_i are the mole fractions of component i in the liquid and solid phases,

132 respectively, and γ_i is the activity coefficient of component i in the mixture. The fugacity

133 ratio $f_i^{\mathrm{S}}/f_i^{\mathrm{L}}$ of the pure component i can be approximately expressed using the melting point

8

134　$(T_{m,i})$ and enthalpy of fusion ($\Delta H_{m,i}$) of the pure component i as follows (Smith et al, 2005):

$$\frac{\gamma_i^L x_i}{\gamma_i^S z_i} = \frac{f_i^S}{f_i^L} = \exp\frac{\Delta H_{m,i}}{RT_{m,i}}\left(\frac{T-T_{m,i}}{T}\right) \tag{2}$$

136　Two assumptions were made when using equation (2) to calculate the liquidus temperature T

137　of a given mixture. The first, which was used in the non-solid-solution model, is that the

138　solid phase consists of a single component ($z_i = 1$, therefore $\gamma_i^S = 1$). This means that

139　different MGs are immiscible in the solid phase. For a binary mixture, the relationship

140　between the mole fraction and liquidus temperature is given by

$$\gamma_1^L x_1 = \exp\frac{\Delta H_{m,1}}{RT_{m,1}}\left(\frac{T-T_{m,1}}{T}\right) \text{ or } \gamma_2^L x_2 = \exp\frac{\Delta H_{m,2}}{RT_{m,2}}\left(\frac{T-T_{m,2}}{T}\right) \tag{3}$$

142　　　　The second assumption, which was used in the solid-solution model, is that different

143　MGs can form a continuous solid solution ($z_i \neq 1$) but the solution is ideal ($\gamma_i^S = 1$). In this

144　case, the liquidus temperature can be determined from the following equation:

$$\left[\gamma_1^L x_1\Big/\exp\frac{\Delta H_{m,1}}{RT_{m,1}}\left(\frac{T-T_{m,1}}{T}\right)\right] + \left[\gamma_2^L x_2\Big/\exp\frac{\Delta H_{m,2}}{RT_{m,2}}\left(\frac{T-T_{m,2}}{T}\right)\right] = 1 \tag{4}$$

146　This is derived from equation (2) and $z_1 + z_2 = 1$. For both models, the activity coefficients in

147　the liquid phase, γ_i^L, were calculated using the UNIFAC (Dortmund) model (Gmehling et al,

148　1993), as in our previous studies (Yoshidomi et al, 2017; Sugami et al, 2017).
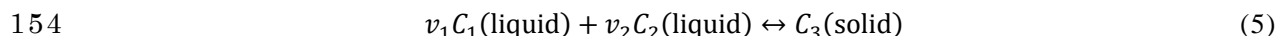
149

150　*Reaction equilibrium*

151　　　　This model assumes that the solidification of MGs is similar to a chemical reaction.

152　When v_1 moles of C_1 and v_2 moles of C_2 in a liquid phase produce a solid compound C_3, the

9

153   reaction is expressed as follows:

$$v_1 C_1(\text{liquid}) + v_2 C_2(\text{liquid}) \leftrightarrow C_3(\text{solid}) \tag{5}$$

155   The reaction equilibrium constant K_a is described by

$$K_a = \frac{(\gamma_1{}^L x_1)^{v_1}(\gamma_2{}^L x_2)^{v_2}}{(z_3)^1} = (\gamma_1 x_1)^{v_1}(\gamma_2 x_2)^{v_2} \tag{6}$$

157   where $\gamma_i{}^L$ and x_i are the activity coefficient and mole fraction of component C_i in the liquid

158   phase, respectively. The term z_3 is the mole fraction of compound C_3 in the solid phase, but

159   because no other solid is present in the system, it can be assumed to be unity. However, there

160   is another expression for the equilibrium constant K_a, which is derived from the Gibbs–

161   Helmholtz equation (Tumakaka et al., 2007):

$$K_a = K_{\text{ref}} \times \exp\frac{\Delta H_{\text{ref}}}{RT_{\text{ref}}}\left(\frac{T - T_{\text{ref}}}{T}\right) \tag{7}$$

163   where K_{ref} and ΔH_{ref} are the equilibrium constant and enthalpy of reaction, respectively, at an

164   arbitrarily chosen reference temperature T_{ref}. By combining equations (6) and (7), we can

165   determine the liquidus temperature T. This model was built according to the method reported

166   by Tumakaka et al. (2007) and is referred to as the compound formation model. The detailed

167   calculation procedure will be described in the following section. It should be noted that v_1

168   and v_2 can be used as fitting parameters in this model. The $\gamma_i{}^L$ terms were estimated by using

169   the UNIFAC (Dortmund) model.

170

171

10

172   **Results and Discussion**

173   Pure component properties

174   All three thermodynamic models involve pure component properties: the melting

175   point T_m and enthalpy of fusion ΔH_m. We therefore used DSC to determine these properties

176   for each pure MG and all crystalline forms; the results are shown in Table 1. We measured

177   three times for each component and chose the middle value. The error ranges were -0.7 ~

178   +1.2 °C for melting point and -14 ~ +10% for enthalpy. The relatively large error for enthalpy

179   might be because of the measurement error of the sample weight (only 10 mg). However, this

180   error did not critically affect the calculation results.

181   The values obtained were consistent with those previously reported (Lutton, 1971;

182   Maruyama et al., 1971; Yoshidomi et al., 2017), therefore we used them for performing

183   calculations with equations (3), (4), and (7). The numbers of functional groups in each MG

184   are also shown in Table 1; they were used to estimate the activity coefficients γ_i^L with the

185   UNIFAC (Dortmund) model.

186

187   Binary MG behaviors

188   Various binary mixtures were analyzed by DSC. Figure 1 shows DSC profiles of the

189   mixture of MG16:0 and MG18:0 for α- and β-type crystals. The endothermic peaks on DSC

190   profiles indicate the phase transition from solid to liquid because melting is an endothermic

11

191   reaction. The liquidus temperature was determined from the endothermic peak maximum

192   temperature for each mixture. Because β-type MG crystal has a higher melting point than that

193   of α-type, the liquidus temperatures of β-type crystal were sifted to higher temperatures than

194   those of α-type.

195   The liquidus temperatures of α- and β-type crystals are shown by solid circles in

196   Figures 2 and 3, respectively, for various binary mixtures of MGs. Each measurement for

197   α-type crystal was conducted twice and the first result was chosen; the absolute deviation

198   between the first and second was within 1.3 °C for any mixtures studied. The β-type crystal

199   was measured once because the sample preparation took four weeks to ensure the transition

200   into β-type.

201   We can obtain the liquidus curves of the binary MGs by connecting these points.

202   The experimental liquidus curves have complex shapes, although we previously reported

203   (Yoshidomi et al., 2017) that binary mixtures of a MG and a FAME give simple, smooth

204   curves. These results imply that the solidification behaviors of MG/MG and MG/FAME

205   mixtures are different. We used the three thermodynamic models described in the previous

206   section to obtain theoretical liquidus curves and compared them with the experimental

207   curves.

208   The theoretical liquidus curves obtained with the non-solid-solution model are

209   shown by dashed-dotted lines in Figures 2 and 3. The model gives v-shaped curves; these

210 correspond to eutectic systems, which are widely found in lipid mixtures (Maximo et al.,

211 2014). The theoretical curves obtained with the solid-solution model are shown by dashed

212 lines. These monotonically increasing curves correspond to solid-solution systems, which are

213 frequently found in binary systems composed of similar elements.

214 Figure 2 shows that the behavior of the α-type crystals depends on the pair of MGs.

215 In the case of the MG12:0/MG18:0 mixture (Figure 2a), because of the difference between

216 the carbon chain lengths ($\Delta C = 6$), the experimental liquidus temperatures are close to those

217 obtained with the non-solid-solution model. In contrast, the MG16:0/MG18:0 pair (Figure 2c;

218 $\Delta C = 2$) conforms to the solid-solution model. These results suggest that a large difference

219 between the carbon chain lengths leads to independent solidification of the individual MGs,

220 whereas similar MGs can form a solid solution. Such a tendency was reported by Maruyama

221 et al. for binary systems of MGs (Maruyama et al, 1978). The behavior of the

222 MG12:0/MG16:0 pair (Figure 2b; $\Delta C = 4$) is intermediate between those indicated by the two

223 models.

224 Figure 3 shows that for β-type crystals, the experimental liquidus curves are close to

225 those obtained with the non-solid-solution model for all pairs, although there are some

226 deviations. The reason for the difference between the behaviors of the α and β crystals

227 remains unclear, but it could arise because of differences among the crystal transition rates of

228 the MGs. In general, a MG with a shorter carbon chain has a shorter transition time

13

229   (Maruyama et al., 1971), therefore MGs with shorter chains will independently change to the

230   β form earlier than the those with longer chains and the solid solution will be disrupted

231   during the crystal transition.

232   The results obtained with the two models based on the solid–liquid equilibrium do

233   not fit the complex shapes of the liquidus curves well. The experimental curves have

234   irregularities, with multiple upward convex lines. We therefore used the compound formation

235   model, which is derived from the reaction equilibrium. The results obtained with this model

236   are shown by solid lines in Figures 2 and 3. These results clearly fit the experimental liquidus

237   curves well.

238   We will use Figure 3c, which is the simplest case, to explain the fitting procedure.

239   We first divided the experimental liquidus curve into three regions (I, II, and III). In regions I

240   and III, the compound formation model exactly matches the non-solid-solution model. This

241   means that only MG16:0 solidifies in region I ($v_1 = 1$, $v_2 = 0$) and only MG18:0 solidifies in

242   region III ($v_1 = 0$, $v_2 = 1$). On the basis of this assumption, the reaction equilibrium constant

243   K_a for each region is $\gamma_1 x_1$ (region I) or $\gamma_2 x_2$ (region III), from equation (6). If the melting

244   point $T_{m,i}$ of the MG is chosen as the reference temperature T_{ref}, the compound formation

245   model, via equations (6) and (7), becomes identical to equation (3) for the non-solid-solution

246   model, i.e., the compound formation model includes the non-solid-solution model as a

247   special case.

14

248   The upward convex curve in region II is thought to indicate compound formation

249   between MG16:0 and MG18:0. For the calculation with equation (7), the highest temperature

250   in the given region was chosen as T_{ref}. The stoichiometric numbers v_1 and v_2 were used as

251   fitting parameters and determined by the least-squares method. The ΔH_{ref} term was estimated

252   as the average of the fusion enthalpies weighted by the stoichiometric numbers, as follows:

253    $$\Delta H_{\text{ref}} = \frac{v_1 \Delta H_{m,1} + v_2 \Delta H_{m,2}}{v_1 + v_2} \qquad (8)$$

254   When $v_1 = 3.63$ and $v_2 = 2.25$, the calculated curve fits the experimental plots well, as shown

255   in Figure 3c. For all cases in Figures 2 and 3, we counted the number of upward convex lines

256   to divide the curves into regions, and then fitting was performed independently for each

257   region in the same way. The obtained parameters are summarized in Table 2. Although we are

258   not certain whether or not the obtained stoichiometric numbers reflect the real world, it can

259   be said that the compound formation model can describe the complex solidification behaviors

260   of MGs.

261   Compound formation in MG mixtures is thought to occur because of the presence of

262   hydroxyl groups, which are involved in hydrogen bonding between MGs. Such strong

263   intermolecular interactions allow easy formation of associated molecules, which can be

264   distinguished by X-ray diffraction (Etter, 1990). Such compound-forming systems have also

265   been reported for triglyceride mixtures (Engström, 1992).

266

15

267   Multi-component mixtures

268   The compound formation model was applied to surrogate biodiesel fuels, namely

269   multi-component mixtures that consisted of MGs and FAMEs. A pair of MGs (1:1 by weight)

270   was added to a mixture of FAME12:0, FAME16:0, and FAME18:1 (65:24:11 by weight) at

271   various MG contents. The liquidus temperatures of the mixtures were determined by DSC,

272   via two methods; the results are shown in Figure 4 by open and solid circles, respectively. We

273   used MG contents higher than 2 wt% because at low contents the MG endothermic peaks in

274   the DSC curves were too weak. Although such high MG contents are rather far from those in

275   real biodiesel, we performed these experiments to investigate the potential of the model.

276   First, we determined the liquidus temperatures, which are shown by open circles in

277   Figure 4, by using the method described in the subsection of analytical method for α-type

278   MGs, in which the sample was immediately reheated after the first exothermic peak was

279   detected on cooling. However, sudden changes in the liquidus temperature can be observed,

280   especially in Figure 4a. This could be caused by the crystal transition from α to β′ or β,

281   because the transition time tends to become shorter in the presence of a solvent. FAMEs can

282   act as a solvent in this case, therefore the MGs sometimes change to the β′ or β type.

283   Determination of the liquidus temperature for α-type MGs in multi-component mixtures is

284   therefore difficult.

285   We therefore modified the DSC method and examined the sample after transition by

286 allowing an adequate transition time. For this purpose, the sample was cooled to −20 °C and

287 then DSC was performed at a heating rate of 3 °C/min. The liquidus temperatures obtained by

288 this method are shown as solid circles in Figure 4. In contrast to the previous results, the

289 liquidus temperatures give monotonous curves. This method enabled us to obtain consistent

290 liquidus curves for β′- or β-type MGs, although the crystal type was not specified in this

291 study.

292   For calculations using the compound formation model, T_{ref} was set at the highest

293 liquidus point among the experimental data. Although the type of crystal was not identified,

294 the enthalpies of fusion for the β type shown in Table 1 were used as tentative values for the

295 calculation. The crystal type is not critical for testing the applicability of the model. The

296 parameters v_1 and v_2 were determined by data fitting to be 0.00 and 1.19 for (a), 0.00 and

297 1.27 for (b), and 0.00 and 0.87 for (c), in Figure 4. The fitting results, which are represented

298 by solid lines, show that the compound formation model works well for predicting the

299 experimental liquidus curves. However, the values of v_1 and v_2 obtained by the model will not

300 always reflect the actual stoichiometric numbers of the solid compounds, because these are

301 just the results of data fittings.

302   The excellent matching of the compound formation model with the experimental

303 data is not surprising because the model has fitting parameters. The compound formation

304 model is therefore an empirical model. In a previous series of studies (Imahara et al., 2006;

17

305   Yoshidomi et al., 2017; Sugami et al., 2017), our ultimate purpose was to establish a

306   non-empirical formula for predicting the behaviors of any biodiesel and blends with fossil

307   diesel. The current study shows the complexity of MGs, even in the case of simple binary

308   mixtures. Although we successfully described the complex liquidus curves by using the

309   compound formation model, the parameters obtained will be useless for other cases because

310   the parameters will change if a different chemical component is used.

311   If the ratio of MGs is fixed, as in Figure 4, the compound formation model can be

312   used to predict biodiesel CFPs. This means that we can develop a formula for predicting the

313   CFPs of biodiesels derived from a feedstock as a function of the MG content by data fitting,

314   as in Figure 4, because the fatty acid composition is almost the same for a given type of

315   feedstock.

316

317   **Concluding remarks**

318   The liquidus temperatures of binary systems of MGs were determined by DSC to

319   investigate their interactions. Three thermodynamic models were applied to the obtained

320   results. The difference between the MG carbon chain lengths (ΔC) affected the liquidus curve

321   shape for α-type crystals. When ΔC was large ($\Delta C = 6$), the liquidus curves were close to

322   those obtained with the non-solid-solution model, in which different MGs solidify

323   independently. When ΔC was small ($\Delta C = 2$), the liquidus curve corresponded to the

18

324   solid-solution model, in which different MGs form a continuous solid solution.

325   These two models based on the solid–liquid equilibrium did not exactly fit the

326   complicated liquidus curves of binary MGs. Only the compound formation model, which is

327   derived from the reaction equilibrium, can describe the complicated behaviors of binary MGs.

328   This implies that the different MGs form a solid compound via intermolecular hydrogen

329   bonding. It was therefore concluded that the compound formation model is appropriate for

330   describing the solidification behaviors of MGs.

331   The suitability of the compound formation model was tested for predicting the

332   behaviors of surrogate diesel fuels that consisted of multi-component mixtures of MGs and

333   FAMEs. The results show that the model represents the liquidus curves well. However, the

334   compound formation model involves fitting parameters, which need to be determined from

335   experimental data. The parameters will change depending on the chemical composition,

336   therefore obtaining general predictions that apply to all cases is difficult. This model only

337   works for biodiesel from known feedstocks. As a next step, we will apply this model to

338   biodiesel fuels derived from various plant oils and establish a prediction formula for each

339   feedstock.

340

341   **Conflict of interest**

342   The authors declare that they have no conflict of interest.

343

344   **References**

345   Chupka, G.M., Yanowitz, J., Chiu, G., Alleman T.L., & McCormick, R.L. (2011). Effect of

346   saturated monoglyceride polymorphism on low-temperature performance of biodiesel.

347   Energy Fuels, **25**:398–405.

348   Chupka, G.M., Fouts, L., Lennon, J.A., Alleman, T.L., Daniels, D.A., & McCormick, R.L.

349   (2014). Saturated monoglyceride effects on low-temperature performance of biodiesel

350   blends. Fuel Process Technol, **118**:302–309.

351   Committee for Standardization Automotive Fuels. (2008). Fatty acid methyl esters (FAME)

352   for biodiesel engines - Requirements and test methods (EN14214). Brussels: European

353   Committee for Standardization (CEN).

354   Coutinho, J.A.P., Gonçalves, M., Pratas, M.J., Batista, M.L.S., Fernandes, V.F.S., Pauly, J., &

355   Daridon, J.L. (2010). Measurement and modeling of biodiesel cold-flow properties.

356   Energy and Fuels, **24**:2667–2674.

357   Dunn, R.O., & Bagby, M.O. (1995). Low-temperature properties of triglyceride-based diesel

358   fuels: Transesterified methyl esters and petroleum middle distillate/ester blends. J Am

359   Oil Chem Soc, **72**:895–904.

360   Dunn, R. (2010). Cold Weather Properties and Performance of Biodiesel. In: The Biodiesel

361   Handbook, 2nd ed. Illinois: AOCS Press.

362   Engström, L. (1992). Triglyceride systems forming molecular compounds. Eur J Lipid Sci

363   Tech, **94**:173–181.

364   Etter, M.C. (1990). Encoding and decoding hydrogen-bond patterns of organic compounds.

365   Acc Chem Res, **23**:120–126.

366   Fischer, E., Bergmann, M., & Barwind, H. (1920). Neue synthese von a-monoglyceriden.

367   Berichte der Dtsch Chem Gesellschaft, 1589–1605. (in German)

368   Gmehling, J., Li, J., & Schiller, M. (1993). A modified UNIFAC model. 2. Present parameter

369   matrix and results for different thermodynamic properties. Ind Eng Chem Res, **32**:178–

370   193.

371   Imahara, H., Minami, E., & Saka, S. (2006). Thermodynamic study on cloud point of

372   biodiesel with its fatty acid composition. Fuel, **85**:1666–1670.

373   Knothe, G. (2005). Dependence of biodiesel fuel properties on the structure of fatty acid

374   alkyl esters. Fuel Process Technol, **86**:1059–1070.

375   Knothe, G., & Dunn, R.O. (2009). A comprehensive evaluation of the melting points of fatty

376   acids and esters determined by differential scanning calorimetry. J Am Oil Chem Soc,

377   **86**:843–856.

378   Lopes, J.C.A., Boros, L., Kráhenbúhl, M.A., Meirelles, A.J.A, Daridon, J.L., Pauly, J.,

379   Marrucho, I.M., & Coutinho, J.A.P. (2008). Prediction of cloud points of biodiesel.

380   Energy and Fuels, **22**:747–752.

381   Lutton, E.S. (1971). The phases of saturated 1-monoglycerides C14-C22. J Am Oil Chem Soc,

382   **48**:778–781.

383   Lutton, E.S., & Jackson, F.L. (1967). Binary systems with monoglycerides. J Am Oil Chem

384   Soc, **44**:357–358.

385   Malkin, T., & Shurbagy, M.R.E. (1936). An x-ray and thermal examination of the glycerides.

386   Part II. The alpha-monoglycerides. J Chem Soc, 1628–1634.

387   Maruyama, T., Niiya, I., Imamura, M., Okada, M., Matsumoto, T., Horisawa, M., &

388   Matsumoto, T. (1971). Study on polymorphism of monoglyceride. I. Transition of crystal

389   modification of 1-monolaurin, 1-monomyristin, 1-monopalmitin, and 1-monostearin. J

390   Japan Oil Chem Soc, **20**:11–18. (in Japanese)

391   Maruyama, T., Niiya, I., Imamura, M., Okada, M., & Matsumoto, T. (1973). Study on

392   polymorphism of monoglyceride. II. Thermodynamic considerations on transition. J

393   Japan Oil Chem Soc, **22**:19–22. (in Japanese)

394   Maruyama, T., Niiya, I., Okada, M., & Matsumoto, T. (1979). Studies on polymorphism of

395   monoglycerides. VIII. Phase behavior of binary monoglycerides systems. J Japan Oil

396   Chem Soc, **28**:26–31. (in Japanese)

397   Maximo, G.J., Costa, M.C., Coutinho, J.A.P., & Meirelles, A.J.A. (2014). Trends and

398   demands in the solid–liquid equilibrium of lipidic mixtures. RSC Adv, **4**:31840–31850.

399   Sarin, A., Arora, R., Singh, N.P., Sarin, R., Malhotra, R.K., & Kundu, K. (2009). Effect of

400   blends of Palm-Jatropha-Pongamia biodiesels on cloud point and pour point. Energy,

23

401   **34**:2016–2021.

402   Smith, J.M., Van Ness, H.C., & Abbott, M.M. (2005). Introduction to chemical engineering

403   thermodynamics, 7th ed. New York: McGraw-Hill Education.

404   Sugami, Y., Yoshidomi, S., Minami, E., Shisa, N., Hayashi, H., & Saka, S. (2017). The effect

405   of monoglyceride polymorphism on cold-flow properties of biodiesel model fuel. J Am

406   Oil Chem Soc, **94**:1095–1100

407   Tang, H., Salley, S.O., & Ng, K.Y.S. (2008). Fuel properties and precipitate formation at low

408   temperature in soy-, cottonseed-, and poultry fat-based biodiesel blends. Fuel, **87**:3006–

409   3017.

410   Tumakaka, F., Prikhodko, I.V., & Sadowski, G. (2007). Modeling of solid–liquid equilibria

411   for systems with solid-complex phase formation. Fluid Phase Equilib, **260**:98–104.

412   Yoshidomi, S., Sugami, Y., Minami, E., Shisa, N., Hayashi, H., & Saka, S. (2017). Predicting

413   solid–liquid equilibrium of fatty acid methyl ester and monoacylglycerol mixtures as

414   biodiesel model fuels. J Am Oil Chem Soc, **94**:1087–1094.

415

416　　**List of Tables**

417　　**Table 1** Thermodynamic properties of MGs

418

419　　**Table 2** Parameters obtained by using compound formation model for various binary

420　　mixtures of MGs and crystalline forms

421

422 **List of Figures**

423 **Fig. 1** DSC profiles of binary mixtures of MG16:0 and MG18:0 for α-type (a) and β-type (b)

424 crystals. (x_1: mole fraction of MG18:0)

425

426 **Fig. 2** Experimental liquidus temperatures for various binary mixtures of α-type MGs and

427 theoretical curves obtained by using the non-solid-solution, solid-solution, and compound

428 formation models

429

430 **Fig. 3** Experimental liquidus temperatures for various binary mixtures of β-type MGs and

431 theoretical curves obtained by using non-solid-solution, solid-solution, and compound

432 formation models

433

434 **Fig. 4** Experimental liquidus temperatures for surrogate biodiesel fuels determined by the

435 method used for α-type MGs (open circles) and modified method (solid circles), along with

436 theoretical curves obtained by using compound formation model (solid lines)

437

Table 1 Thermodynamic properties of monoglycerides

Component and type of crystal		Melting point, °C	Enthalpy of fusion, kJ/mol	Number of UNIFAC functional group					
				CH_3	CH_2	CH	OH(p)	OH(s)	CH_2COO
MG12:0	α	44.4	22.4	1	11	1	1	1	1
(1-monolaurin)	β	62.1	47.5						
MG16:0	α	64.9	34.4	1	15	1	1	1	1
(1-monopalmitin)	β	72.8	67.1						
MG18:0	α	71.6	35.1	1	12	1	1	1	1
(1-monostearin)	β	78.9	75.2						

Table 2 Parameters obtained by using compound formation model for various binary mixtures of MGs and crystalline forms

Number of regions	Parameters	C_1 = MG12:0 C_2 = MG18:0		C_1 = MG12:0 C_2 = MG16:0		C_1 = MG16:0 C_2 = MG18:0	
		α	β	α	β	α	β
1	T_{ref}, °C	44.4	62.1	44.4	62.1	64.9	72.8
	v_1	1.00	1.00	1.00	1.00	1.00	1.00
	v_2	0.00	0.00	0.00	0.00	0.00	0.00
2	T_{ref}, °C	46.6	62.9	43.9	60.7	66.8	72.4
	v_1	0.79	2.11	0.002	0.18	0.74	3.63
	v_2	0.50	1.12	0.07	0.32	0.07	2.25
3	T_{ref}, °C	57.4	73.7	47.2	64.2	67.5	78.9
	v_1	0.65	0.10	1.19	0.44	0.23	0.00
	v_2	1.22	2.24	0.81	1.11	0.21	1.00
4	T_{ref}, °C	70.6	71.6	54.4	71.7	70.9	-
	v_1	0.18	0.00	1.44	0.20	0.09	-
	v_2	1.37	1.00	2.39	3.17	0.57	-
5	T_{ref}, °C	71.6	-	64.9	72.8	71.6	-
	v_1	0.00	-	0.00	0.00	0.00	-
	v_2	1.00	-	1.00	1.00	1.00	-

Fig. 1

Fig. 2

Fig. 3

Fig. 4